

# RSC Advances

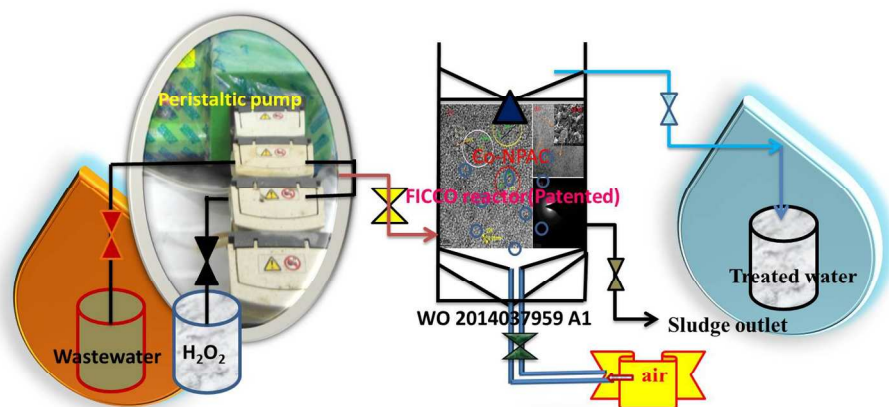


This is an *Accepted Manuscript*, which has been through the Royal Society of Chemistry peer review process and has been accepted for publication.

*Accepted Manuscripts* are published online shortly after acceptance, before technical editing, formatting and proof reading. Using this free service, authors can make their results available to the community, in citable form, before we publish the edited article. This *Accepted Manuscript* will be replaced by the edited, formatted and paginated article as soon as this is available.

You can find more information about *Accepted Manuscripts* in the [Information for Authors](#).

Please note that technical editing may introduce minor changes to the text and/or graphics, which may alter content. The journal's standard [Terms & Conditions](#) and the [Ethical guidelines](#) still apply. In no event shall the Royal Society of Chemistry be held responsible for any errors or omissions in this *Accepted Manuscript* or any consequences arising from the use of any information it contains.



Mechanistic view for degradation of dye laden wastewater  
298x138mm (150 x 150 DPI)

**Synthesis characterization of Co-NPAC and insitu hydroxyl radical generation for  
oxidation of dye laden wastewater from leather industry**

**S.Karthikeyan<sup>a</sup>, R. Bavas Ahamed<sup>b</sup>, M. Velan<sup>b</sup>, G.Sekaran<sup>a\*</sup>**

*a. Environmental Technology Division, Council of Scientific and Industrial Research (CSIR)*

*- Central Leather Research Institute (CLRI), Adyar, Chennai-600 020, Tamilnadu, India.*

*b. Chemical Engineering Department, Anna University, Guindy, Chennai 600 025 Tamil  
Nadu, India*

**\* Corresponding Author**

**Dr. G. Sekaran,**

Chief Scientist & Cluster chairman

Environmental Technology Division,

Central Leather Research Institute,

Adyar, Chennai – 600 020,

Tamil Nadu, India

Tel.: +91-44-24911386 (Extn: 7141)

Fax: +91-44-24452941

**Email: ganesansekar@gmail.com**

**Abbreviations**

|                  |  |
|------------------|--|
| APHA             | American Public Health Association               |
| AOP              | Advanced oxidation process                       |
| NPAC             | Nanoporous Activated Carbon                      |
| Co-NPAC          | Cobalt oxide on Nanoporous Activated Carbon      |
| BET              | Brunauer-Emmett-Teller                           |
| HK               | Horvath Kawazoe                                  |
| XPS              | X-ray Photoelectron Spectroscopy                 |
| EES              | Excitation Emission Spectra                      |
| HR-TEM           | High resolution-Transmission Electron Microscopy |
| HR-SEM           | High resolution-Scanning Electron Microscopy     |
| XRD              | X-Ray Diffraction                                |
| EPR              | Electron Paramagnetic Resonance                  |
| EDX              | Energy-Dispersive X-ray spectroscopy             |
| ROS              | Reactive Oxygen Species                          |
| COD              | Chemical Oxygen Demand                           |
| TOC              | Total Organic Carbon                             |
| BOD <sub>5</sub> | Biological Oxygen Demand                         |

**Abstract**

Cobalt oxide supported nanoporous activated carbon (Co-NPAC) could be utilized as a catalyst in heterogeneous Fenton oxidation of organic dye chemicals in tannery wastewater. The nanoporous activated carbon (NPAC) was prepared from rice husk by precarbonization followed by chemical activation at elevated temperature. The Co-NPAC was characterized by UV-visible, Fluorescence spectroscopy, FT-IR, TEM, XRD, BET surface area and XPS analysis. The role of Co-NPAC in generating hydroxyl radical from hydrogen peroxide was verified using  $\lambda_{\text{exi}}$  and  $\lambda_{\text{emi}}$  at 320nm and 450nm respectively from Excitation Emission Spectra (EES). The parameters for the treatment of dye laden tannery wastewater such as dosage of Co-NPAC and concentration of  $\text{H}_2\text{O}_2$ , pH and temperature were optimized. The refractory organic compounds estimated in terms of chemical oxygen demand (COD), in tannery wastewater were eliminated during hetero Fenton like a process by 78%. The characterization of the wastewater before and after heterogeneous Fenton oxidation was confirmed using UV-Visible spectra, EES, and FT-IR spectra. The Co-NPAC retained catalytic activity upto 5 cycles with sustained generation of hydroxyl radicals.

**Keywords:** Nanoporous activated carbon, Heterogeneous Fenton resembling catalyst, Tannery wastewater, Hydroxyl radical, Organic dyes.

## Introduction

In India, there are more than 3000 tanneries classified under small scale to medium scale sectors. Leather industries generate wastewater containing natural and synthetic organic dyes, syntans, organic nitrogen, ammonical nitrogen, sulphates, sulfides and heavy metals<sup>1</sup>. Wastewater generated from leather industry contains significant concentration of refractory organic compounds and hazardous pollutants<sup>2</sup>. The unit operations such as primary treatment, secondary biological treatments, tertiary treatment processes. Nano filtration and reverse osmosis are generally used after tertiary treatment to recover water from treated tannery wastewater<sup>3</sup>. Biological treatment using aerobic and anaerobic microbes is employed to oxidize the organics in wastewater. However, the chromophoric (organic dyes) present in the tannery wastewater escape the biological treatment processes without degradation. The tertiary treatment process such as UV assisted catalytic oxidation, ultrasound induced processes and electrical energy mediated oxidizing processes are being employed for the removal of bio resistant organic dye chemicals in biological treated tannery wastewater<sup>4,5</sup>. Amongst tertiary treatment processes, advance oxidation processes gained their importance to eliminate refractory organics in treated tannery wastewater and Fenton oxidation processes has been under commercial exploitation<sup>6</sup>. However, it is associated with the formation of ferric hydroxide sludge formation, which may be regarded as serious disadvantage<sup>7</sup>. To overcome these serious drawbacks and to facilitate the Fenton reaction at neutral pH conditions many developments have been emerged such as replacing the ferrous ion by other heavy metal ions oxidizing agents such as ozone, oxygen, air, hypochlorite instead of H<sub>2</sub>O<sub>2</sub> were also applied to modify homogeneous Fenton oxidation process<sup>8</sup>. Other forms of Fenton process had been developed by many researchers for the oxidation of organics in wastewater such as electro Fenton and photo Fenton processes. They were integrated with short comings such as substantial amount of energy consumption besides considerable expenditure on

chemicals. Energy intensive technologies for the treatment of wastewater have been not well appreciated by end users due to shortage of electrical power even though sustained requirement for environmental management. Recently heterogeneous catalytic oxidation process has been reported to overcome the issues addressed in conventional homogeneous Fenton oxidation processes<sup>9</sup>. TiO<sub>2</sub>/Si-C composite was used as a catalyst in an advanced oxidation process for the degradation of methylene blue, phenol, naphthalene, and abamectin from coal mine effluent<sup>10</sup>. Iron impregnated polyacrylamide (IIPA) powder catalyst was used as heterogeneous catalyst for the oxidation of organics in municipal wastewater with minimum sludge production of 20mg/gCOD destructed<sup>11</sup>. Iron doped TiO<sub>2</sub> coated over activated carbon (FTA) exhibited better efficiency than their individual elements/compounds in UV- photo catalysis besides it's economically viable<sup>12</sup>. Gold was impregnated in ferric oxide, titanium dioxide or in activated carbon for the oxidative degradation of bisphenol-A<sup>13</sup>,<sup>14</sup>. Au-Pd bimetallic nanoparticle impregnated tubular mesoporous activated carbon was used as highly dispersed nano catalyst for the treatment of refractory organics in wastewater<sup>15</sup>. In advanced oxidation process activated carbon supported cobalt catalyst using peroxymonosulphate as an oxidizing agent removed phenol very efficiency<sup>16</sup>. Yang et al. investigated Al<sub>2</sub>O<sub>3</sub>, TiO<sub>2</sub> and SiO<sub>2</sub> supported cobalt catalysts for the degradation of 2, 4-dichlorophenol in waste water<sup>17, 18</sup>. The supported Co catalysts showed efficiency in the order Co/SiO<sub>2</sub> > Co/TiO<sub>2</sub> > Co/Al<sub>2</sub>O<sub>3</sub><sup>19</sup>. Carbon black composites (CBC) impregnated with Pt, Pd and Ru catalysts were used in wet air oxidation of phenol<sup>20</sup>. Hydrated ferric oxide doped activated carbon fiber was used for the adsorption of phosphate<sup>21, 22</sup>. Carbon supported nano aggregated Pt (Pt/C) was used for efficient oxidation of isopropyl alcohol in wastewater with efficiency 99.7%<sup>23</sup>. The heterogeneous Fenton like catalysts were efficient enough for the degradation of synthetic organic compounds in wastewater. However, reports on heavy metal impregnated Fenton resembling catalyst for the oxidation of organic dye compounds in

tannery wastewater are very less or perhaps nil. Hence, the focal theme of the present investigation was on synthesis and characterization of Co-NPAC, and application to the heterogeneous Fenton oxidation of organic dye compounds in tannery effluent.

### **Materials and methods**

Tannery wastewater for the present investigation was collected from a common effluent treatment plant (CETP) catering to tannery cluster in Chennai, Tamil Nadu, India. Chemicals and reagents used in this study were laboratory standard bought from SIGMA-ALDRICH.

### **Preparation of NPAC**

This involves precarbonization followed by chemical activation. During precarbonization the rice husk was heated to 400 °C for 4h under N<sub>2</sub> atmosphere and cooled down to room temperature. The precarbonised rice husk of weight 50g carbon was subjected to chemical activation using phosphoric acid, 250 g containing 85% H<sub>3</sub>PO<sub>4</sub> (w/w). The effect of H<sub>3</sub>PO<sub>4</sub> is to produce chemical changes and structural alterations in the porous activated carbon surface. Phosphoric acid functions in two ways. The first aspect is to promote bond cleavage reaction of precarbonized material due to its acidity and to combine with organic species to form phosphate linkages, such as phosphate esters. They were mixed uniformly at 85 °C for 4 h. After drying the mixture at 110 °C, it was again heated under N<sub>2</sub> atmosphere at 800 °C for 4 h. Then it was washed for several times using hot water for several times and finally with cold water to remove unspent phosphoric acid and it was followed by drying at 110 °C<sup>24</sup>.

### **Preparation of cobalt oxide on nanoporous activated carbon (Co-NPAC)**

The Co-NPAC was prepared by treating the NPAC with cobalt nitrate solution followed by thermal activation at an elevated temperature. The nanoporous activated carbon (50g) prepared by method discussed with above section was mixed with cobalt nitrate solution (cobalt nitrate dissolved in concentrated nitric acid) for the cobalt nitrate solution of different concentration (0.1wt. % - 2wt. %). Sodium-borohydride ( $\text{NaBH}_4$ ) was added to the mixture and agitated at 85 °C for 8 h. After drying at 110 °C, it was heated at 550 °C for 5 hours. The prepared catalyst was washed with distilled water for several times. It was dried again at 110 °C and milled well to obtain cobalt oxide on nanoporous activated carbon (Co-NPAC) of size 300 $\mu$ .

### **Characterization of NPAC and Co-NPAC**

The synthesized Co-NPAC was characterized physical and chemical properties. The Co-NPAC was examined by X-ray photoelectron spectroscopy (XPS) was carried out in a SPECS XPS system using 150 W Al-K $\alpha$  radiations. The 2p core level spectrum of Co and 1s core level spectra of C, N and O were obtained at 25 eV pass energy. XPS analysis was carried out to confirm the oxidation states of the elements in the prepared samples. The BET surface area was measured by  $\text{N}_2$  adsorption isotherm at 77 K using QUADRASORB (SI) automated surface area and pore size analyzer (Quantachrome Corporation, USA). Brunauer-Emmett-Teller (BET) and Horvath Kawazoe (HK) methods were used to calculate surface area and pore size distribution in NPAC and Co-NPAC. The FT-IR Spectroscopy (Perkin-Elmer) was used for the investigation of the surface functional groups in NPAC and Co-NPAC were recorded in the range of 4000 to 400  $\text{cm}^{-1}$  for 20 scans. NPAC and Co-NPAC samples weight of 0.1 g were mixed with, spectroscopy grade KBr of 1g (Merk, Darmstadt, Germany), the NPAC and Co-NPAC samples with KBr were pelletized (circular) with

dimensions, thickness; 1mm and diameter; 13 mm with spectroscopic standard KBr in a mortar. Part of this mix was introduced in a cell connected to a piston of a hydraulic pump giving a compression pressure of 15 kPa / cm<sup>2</sup>. The UV–Vis spectroscopy to measure the absorbance wavelength of Co-NPAC Fenton oxidation of dye laden tannery wastewater samples before and after were performed on a Varian, CARY 100C double beam spectrophotometer using 1 cm quartz cuvette and scanned in the range of  $\lambda_{200}$  to 800 nm. The elemental composition (carbon, hydrogen and nitrogen) of Co-NPAC was determined using Vario MICRO CHNSO 15091002 (model Carlo–Erba analyser. The technique involves combustion of test sample in an oxygen rich environment. The products of combustion in a CHNS analysis (CO<sub>2</sub>, H<sub>2</sub>O, N<sub>2</sub> and SO<sub>2</sub>) were carried through the system using He as carrier gas. The photoluminescence spectra to determine the excitation and emission wavelengths of initial and after Co-NPAC treated wastewater were measured using Varian Cary eclipse (ELO7023695) fluorescence spectrophotometer with an excitation source from Xe lamp in the wavelength range of 350 – 700 nm. The Thermo Gravimetric Analysis (TGA) was carried out under nitrogen atmosphere from 30 to 800°C, with a temperature gradient of 20°C/min and scans were recorded using TGA Q50 (V20.6 Build 31). The HR-TEM images were recorded using TECNAI (PHILIPS, and Netherlands). The crystalline structural properties were examined using XRD Rich Siefert 3000 diffractometer under Cu K $\alpha$ 1 radiation ( $\lambda=1.54$  A°). The surface morphology of Co-NPAC was determined using a Quanta 200 FEG high resolution Scanning Electron Microscope (SEM).

### **Optical analysis of initial and treated effluent**

Wastewater was analyzed before and after treatment using UV-Visible spectrophotometry (Varian/ CARY 100C) in the range of  $\lambda_{800-200}$  nm using path length of 1cm. Fluorescence excitation/emission spectra of the initial and treated samples were

recorded using Fluorescence spectrophotometry (Varian/ CARY) under 3D mode with the excitation wavelength ranging from 200 to 420nm using quartz cuvette of path length 1cm. FT-IR spectra (Perkin-Elmer) were recorded for the wastewater samples before and after treatment in the range of 4000 to 400  $\text{cm}^{-1}$  for 20 scans using potassium bromide (KBr) as background. The samples were prepared by drying at 110<sup>0</sup>C and pelletized (circular) with dimensions, thickness, 1mm and diameter, 13mm using spectroscopic standard KBr.

### **Heterogeneous Fenton oxidation of dye laden tannery wastewater**

Heterogeneous Fenton oxidation of dye laden tannery wastewater using Co-NPAC was studied under batch mode. Tannery effluent of volume 200 ml was taken and 1g of Co-NPAC was added to it along with hydrogen peroxide (30%w/v). Compressed air at a pressure of 0.6kg/m<sup>2</sup> for 5h was passed into the content of the batch reactor. The oxidation process was optimized for catalyst concentration in terms of cobalt in Co-NPAC were (0.1wt.%, 0.5wt.%, 1.0 wt.%, 1.5 wt.% and 2 wt.%), H<sub>2</sub>O<sub>2</sub> dosage (2mM, 4mM, 6mM, 8mM and 10mM), temperature (25 °C, 45 °C and 55 °C) and pH (3, 4, 5, 6, 7, 8, 9 and10) at different hydraulic residence time. The amount of cobalt in Co-NPAC before and after treatment with tannery wastewater was determined using Atomic Absorption Spectrophotometer (Shimadzu AA 6650). The characteristic of wastewater before and after heterogeneous Fenton oxidation are presented in Table 1

### **H<sub>2</sub>O<sub>2</sub> estimation**

The concentration of H<sub>2</sub>O<sub>2</sub> was estimated by iodometric method. The concentration of H<sub>2</sub>O<sub>2</sub> was determined at an interval of 30 min upto 7 hours in four different experiments. The oxidation of dye laden wastewater was attempted in varied experiments and they were heterogeneous Fenton oxidation using Co-NPAC as a catalyst at pH7, Homogeneous Fenton

using  $\text{FeSO}_4 \cdot 7\text{H}_2\text{O}$  and  $\text{H}_2\text{O}_2$  at pH 3.5 and pH 7, control studies in the presence of only  $\text{H}_2\text{O}_2$  and in the presence of only Co-NPAC<sup>25</sup>.

### Confirmation of hydroxyl radical formation by EES

Generation of hydroxyl radical in the presence of catalyst could be identified from fluorescence emission spectrum using Terephthalic acid (TPA) as standard, TPA combines with hydroxyl radical to form 2-hydroxyterephthalic acid which is fluorescent active at emission of  $\lambda_{425\text{nm}}$  with excitation at  $\lambda_{315\text{nm}}$ <sup>26</sup>. The hydroxyl radical generation potential of Co-NPAC was assessed by confining the radicals with TPA; 1g of Co-NPAC was added to TPA along with 5mM of  $\text{H}_2\text{O}_2$  to generate the hydroxyl radical. The samples were analyzed by fluorescence spectrophotometer (Varion/ CARY) at different time intervals in the excitation< $\lambda$ > range between 200nm to 540nm for the emission< $\lambda$ > search from 210nm to 800nm.

### Reusable characteristic of Co-NPAC

The reusability of Co-NPAC for the oxidation of dye laden tannery wastewater was studied by applying the same catalyst for 5 cycles with same hydraulic residence time of 9 h. At the end of each cycle the catalyst was filtered using whattman No.1 filter paper and dried well before applying to the next cycle containing the same volume of fresh effluent. The utilization of  $\text{H}_2\text{O}_2$  by the catalyst to form hydroxyl radical was studied for five successive cycles.

### Results and discussion

The XRD spectra of NPAC and Co-NPAC are shown in Fig.1a. The d-spacing of  $\text{Co}_3\text{O}_4$  was calculated to be 0.45 nm, corresponding to characteristic (111) plane in cobalt oxide (JCPDS 43-1003)<sup>27</sup>. The d-spacing in  $\text{Co}_2\text{O}_3$  and CoO were 0.32 and 0.25 nm

respectively as reported<sup>27</sup>. This confirms that  $\text{Co}_3\text{O}_4$  was the dominant phase in the cobalt oxide on NPAC matrix. These results are consistent with the results from the XRD characterization. XPS data of cobalt oxide supported on nanoporous activated carbon are presented in Fig. 1b. The observed  $\text{Co}2p_{1/2}$  and  $\text{Co}2p_{3/2}$  peaks in Co-NPAC with binding energies of about 781 eV and 796 eV were characteristic of  $\text{Co}_3\text{O}_4$  species. The  $\text{O}1s$  for oxygen is observed at a binding energy of 531.4 eV. It could be seen that two separated 2p electron orbital energy states of  $\text{Co}2p_{3/2}$  and  $\text{Co}2p_{1/2}$  peaks centered at 781 eV and 796 eV<sup>29</sup>, with the binding energy difference of 15 eV. This indicates that cobalt mainly exists as cobalt oxide in the nanoporous activated carbon matrix.  $\text{Co}_3\text{O}_4$  was identified by the binding energies, peak shape, spin-orbital splitting of 15 eV, and the absence of intense satellite structure. The ( $\text{Co} 2p_{1/2}$ –  $\text{Co} 2p_{3/2}$ ) energy separation is approximately 15.3 eV, which corresponds to the pure phase of  $\text{Co}_3\text{O}_4$  as reported in the literature<sup>30</sup>. Thus, XPS data are in agreement with XRD characterization (Fig. 1a). Both the characterizations suggest that  $\text{Co}_3\text{O}_4$  particles of almost the same diameter represent dominant cobalt oxide in the matrix<sup>31</sup>.

The thermal stability of NPAC and Co-NPAC was investigated using TGA analysis and their TGA curves are shown in Fig. 1c. NPAC and Co-NPAC exhibited a huge weight loss (11.62%) at about 100 °C–200 °C due to removal of moisture content and bound water molecules from NPAC matrix<sup>32</sup>. In contrast, NPAC and Co-NPAC exhibited a very less weight loss at 200 °C, may be attributed to simultaneous melting of the precursor and continuous denitration of remaining nitrates from cobalt precursor. However, both of them showed a weight loss by 11% in the temperature range of 300–538 °C. This was attributed to the decomposition of the carbon network structure leading to a major release of carbon containing gaseous products (mostly  $\text{CO}_2$ ,  $\text{CO}$ ,  $\text{C}_6\text{H}_6$  and a small amount of  $\text{H}_2$  and hydrocarbon mixtures) and formation of cobalt oxide ( $\text{Co}_3\text{O}_4$ ). The third stage loss of mass in

NPAC and Co-NPAC occurred at 800 °C, this may be attributed to the release of CO<sub>2</sub> and CO owing to reduction of CoO by carbon.

The integration of cobalt oxide with nanoporous activated carbon was confirmed by FT-IR spectroscopy as shown in Fig.1d. The IR peaks at 2935 cm<sup>-1</sup> and 2925 cm<sup>-1</sup> are due to C-H stretching in NPAC and Co-NPAC. The stretching frequency at 3408 cm<sup>-1</sup> is attributed to the NH<sub>2</sub> group which was shifted by 26 cm<sup>-1</sup>, possibly by the interaction of non-bonded electrons in nitrogen with cobalt in the Co-NPAC matrix. Characteristic peaks at 1621cm<sup>-1</sup> and 1109 cm<sup>-1</sup>, were appeared in both these spectra that may be assigned to the asymmetric and symmetric carboxylate stretching functional groups in the NPAC. The peaks at 1621cm<sup>-1</sup> and 1109 cm<sup>-1</sup> in NPAC have slightly shifted to 1645 cm<sup>-1</sup> and 1069 cm<sup>-1</sup> in Co<sub>3</sub>O<sub>4</sub> sample, indicating the interaction with the surface of the Co<sub>3</sub>O<sub>4</sub> sample. XPS spectrum also confirmed the carboxylate functional groups in the carbon matrix. The two characteristic bands at 585 cm<sup>-1</sup> and 669 cm<sup>-1</sup> originating from the stretching vibrations of the metal oxygen bonds may be assigned to Co<sub>3</sub>O<sub>4</sub>. The first band at 585 cm<sup>-1</sup> is associated with the cobalt (III) oxide vibration. The band at 669 cm<sup>-1</sup> originates from the cobalt (II) oxide vibration. The pore dimension, pore size distribution and pore volume for NPAC and Co-NPAC are presented in Fig.2a and 2b. The total surface area, meso pore surface area, micropore surface area, total pore volume, micro pore volume, meso pore volume and pore diameter (6nm) of the samples are shown in Table 2. The BET surface area values were evaluated to be 153 m<sup>2</sup>/g, 52 m<sup>2</sup>/g for NPAC and Co-NPAC respectively. The total pore volume was evaluated to be 0.19cm<sup>3</sup>/g for the same samples. The total surface area was decreased for cobalt oxide in the NPAC. Total surface area, mesopore surface area and macropore surface area are the lowest for Co-NPAC. The total pore volume decreased after supporting with cobalt oxide. The cobalt oxide was supported with in the pores of NPAC leading to lowering of surface area as observed in SEM. The lowering of surface area of Co-

NPAC is mainly due to the packing of cobalt oxide in the pores. The SEM images of Co-NPAC show the uniformly anchored NPAC matrix (Fig.3a, c), and both kinds of porous structures are well preserved. The EDX analysis uncovered, however, that the cobalt oxide particles encapsulated inside nanoporous activated carbon containing silicon (Fig. 3d), while the cobalt oxide nanoparticles are principally situated in the NPAC matrix. Cobalt oxide spheres supported nanoporous activated carbon was investigated at the nano-scale level using HRTEM (Fig. 4a, b). Particles with higher electron density were detected both inside and outside of nanoporous activated carbon matrix and the selective area electron diffraction (SAED) images to investigate the microstructure of the catalyst (Fig.4c). The HR-TEM and XRD patterns (Fig. 5a, b) and SAED pattern show the polycrystalline nature of NPAC (Fig.5c). Fig. 6a-f HRTEM images show that the cobalt oxide particles of different size (nanometer) were anchored to the irregular shaped graphitic crystallites of NPAC matrix.

#### **Catalytic oxidation of dye laden wastewater using cobalt oxide supported nanoporous activated carbon**

The heterogeneous Fenton oxidation process was carried out at different reaction conditions such as varied catalyst concentration, variation in H<sub>2</sub>O<sub>2</sub> dosage, various pH and temperature. Decrease in COD of the wastewater with increase in time was used to evaluate the kinetics of advanced oxidation process. Five different mass percent (0.1wt %-2 wt %) of Co-NPAC were employed in advanced oxidation process with 10mM of H<sub>2</sub>O<sub>2</sub> by keeping other parameters constant. The oxidation reaction mainly depends on the available active sites in NPAC, the added H<sub>2</sub>O<sub>2</sub> and the volume of tannery effluent. The reaction was assumed to follow pseudo second order kinetics and its mathematical equation is

$$1/C_t = kt + 1/C_0 \quad (1)$$

Where, ' $C_0$ ' is initial COD of the tannery effluent, ' $C_t$ ' is the COD of the effluent at time ' $t$ ' and ' $k$ ' is the rate constant. **Fig. S1a, b** present that the reaction rate constant,  $k$  was  $5.54 \text{ Lkg}^{-1}\text{min}^{-1}$  with cobalt mass percentage of 1wt.% and it had the highest  $R^2$  value of 0.9807 for the plot  $1/C_t - 1/C_0$  versus time,  $t$ . The reaction rate was lower at smaller mass percent of cobalt oxide in Co-NPAC catalyst, 1wt. %, and due to lack of catalyst. The rate constant values are shown in Table S1. The  $\text{H}_2\text{O}_2$  added into the reaction favored in all the cases with respect to the availability of catalyst's active sites. At higher mass percent cobalt oxide in NPAC, above 1wt. %, the reaction rate was lowered, may be due to the accumulation of large amount of cobalt oxide leads to the shielding of active sites themselves. The reduction in active site accessibility led to decrease in the reaction rate with 1.5 wt. % and 2wt. % of Co-NPAC. Fig. 7 shows COD reduction due to adsorption by Co-NPAC was only 16%, in homo Fenton oxidation using  $\text{FeSO}_4 \cdot 7\text{H}_2\text{O}$  and  $\text{H}_2\text{O}_2$  was, 65.32%, in heterogeneous Fenton using Co-NPAC at pH 7 was 78%. The percentage reduction in COD was less in the absence of Co-NPAC and  $\text{H}_2\text{O}_2$ .

In heterogeneous Fenton oxidation process the amount of  $\text{H}_2\text{O}_2$  added was varied from 2mM to 10mM. Fig. 8a and Fig. 8b show the reaction rate constant was  $5.68 \text{ Lkg}^{-1}\text{min}^{-1}$  in the presence of  $\text{H}_2\text{O}_2$  @ 10mM and it obeyed the pseudo second order rate with  $R^2$  value of 0.9822. Table S2 presents the pseudo second order rate constant,  $k$  and  $R^2$  values at different dosages of  $\text{H}_2\text{O}_2$ . The reaction rate was increased with increase in substrate concentration. Further increase in the  $\text{H}_2\text{O}_2$  might increase the reaction rate, but the COD was apparently increased due to the residual  $\text{H}_2\text{O}_2$  in the reactor. As reported that the Fenton reaction was highly active only at acidic pH around 3.5<sup>33</sup>, the heterogeneous Fenton process was studied at different pH values from 3 to 10 with 5mM of  $\text{H}_2\text{O}_2$ . Fig. 9a and Fig. 9b show the maximum reaction rate constant was  $4.05 \text{ Lkg}^{-1}\text{min}^{-1}$  at pH 3. **Table S3** shows that the pseudo second order rate constant of heterogeneous Fenton oxidation process with

(a)

corresponding  $R^2$  values at different pH. The scavenging activity at the active sites of the catalyst was increased and the corresponding reaction rate was decreased in the presence of concentration of  $\text{OH}^-$  increased in the reaction mixture. The relatively low concentration of  $\text{OH}^-$  ions in acidic medium results in the faster rate of formation of hydroxyl radical, and the rate of reaction decreased with increase in pH for the constant dosage of  $\text{H}_2\text{O}_2$ . However, the reaction obeyed pseudo second order reaction kinetics with  $R^2$  value of 0.98. The reaction rate could be increased even at natural pH of the effluent, 7.8 by increasing  $\text{H}_2\text{O}_2$  concentration. Fig. 10a and Fig. 10b show the effect of reaction temperatures on the oxidation of dye compounds in tannery effluent. The reaction proceed with lower reaction rate constant of  $4.8\text{Lkg}^{-1}\text{min}^{-1}$  at  $25^\circ\text{C}$ . **Table S4** showed the pseudo second order kinetics of heterogeneous Fenton process and corresponding  $k$  (reaction rate) and  $R^2$  values at different temperatures,  $45^\circ\text{C}$  and  $55^\circ\text{C}$ . The rate of reaction was increased as the temperature was increased with range from  $45^\circ\text{C}$  to  $55^\circ\text{C}$ . The increase in thermal energy helped in the higher mass transfer rate across liquid-solid interface. The movement of  $\text{H}_2\text{O}_2$  to the catalyst active site from solution and the discharge of generating hydroxyl radical into the solution from solid boundary are increased at the elevated temperatures. The reaction rate was increased to  $4.91$ ,  $4.96$  and  $6.41\text{Lkg}^{-1}\text{min}^{-1}$  at  $35^\circ\text{C}$ ,  $45^\circ\text{C}$  and  $55^\circ\text{C}$  respectively.

### **Confirmation of heterogeneous Fenton oxidation of dye compounds in tannery wastewater**

#### **UV-Visible spectrophotometer**

The UV-Vis spectra of wastewater before and after Fenton oxidation were recorded in the wavelength range of 200 to 800 nm. The initial raw tannery effluent was turbid and black in color the wastewater exhibited strong absorption on the visible region and with optical density 0.6. The Fenton oxidized wastewater did not show any significant absorbance

over the visible light region and had no considerable intensity in color. But there was no significant change in absorbance in the UV range from  $\lambda_{220}$  to  $\lambda_{230}$  nm and from  $\lambda_{260}$  to  $\lambda_{290}$  nm. The intense peak at  $\lambda_{229}$  nm in raw wastewater before Fenton oxidation may be attributed to aromatic compounds having benzene ring in its structure<sup>34</sup> and it was reduced significantly after treatment with Co-NPAC and treatment only with  $H_2O_2$ . The peak at  $\lambda_{229}$  nm, the corresponding compound, was eliminated during oxidation with Co-NPAC catalyst. The change in pattern of UV-Visible spectrum as a function of time was recorded for the tannery wastewater sample before and after heterogeneous Fenton oxidation, as shown in Fig. 11a and Fig. 11b. As the reaction progress the degradation of organic compounds in wastewater was continued and thus the absorbance was reduced with time due to decrease in concentration of pollutants. The disappearance of peak started with the laps of reaction time of 60 minutes. At the end of 300 minutes, the peak disappeared completely and the wide hump at 280 nm, due to phenolic compound, was reduced to minimum intensity.

### Fluorescence spectrophotometry

The excitation and emission spectra of initial and Fenton oxidized tannery effluent was recorded in the wavelength range from  $\lambda_{200}$  to 400 nm due to excitation and at  $\lambda_{200}$  to 800 nm due to emission. In Fig. 11c the tannery effluent before Fenton oxidation has the emission wavelength in the range from  $\lambda_{330}$  to 370 nm ( $\lambda_{max}$  350nm) and excitation wavelength was at 280 nm. The treated effluent has wide range of emission from  $\lambda_{370}$  to 500 nm ( $\lambda_{max}$  430nm) and excitation at 325 nm, and the overall intensity of the treated wastewater was reduced significantly compared to intensity for dye laden tannery wastewater before treatment (Fig. 11d).

### FT-IR spectroscopy

Fig.S2 shows the FT-IR spectra of tannery effluent sample before and after catalytic oxidations. The  $\text{-O-H-}$  stretch at wavenumber of  $3440\text{ cm}^{-1}$ , is due to the hydroxyl group in phenolic compounds of the dye laden tannery wastewater. This was absent in the homogeneous and heterogeneous Fenton oxidation of tannery effluent. The linked peaks at wavenumbers  $2954\text{ cm}^{-1}$  and  $1436\text{ cm}^{-1}$  (multi peaks) are attributed to the presence of  $\text{-C-H-}$  stretch and  $\text{-C=C-}$  stretching vibration respectively, due to aromatic compounds and they were completely absent in the effluent after Fenton oxidation process. Initial effluent shows  $\text{-C=O-}$  stretch due to amide group at  $1656\text{ cm}^{-1}$ ,  $\text{-C-O-}$  stretch due to ether at  $1120\text{ cm}^{-1}$  and  $\text{-C-Cl-}$  stretch due to alkyl halide at  $626\text{ cm}^{-1}$ . A slight peak at  $2430\text{ cm}^{-1}$  in tannery wastewater after Fenton oxidation is due to non-symmetrical alkane  $\text{-C-H-}$  stretch and the peak at  $1638\text{ cm}^{-1}$  shows the unsaturated  $\alpha, \beta$  carbon stretch<sup>35</sup>. The results of UV-Visible spectra, excitation and emission spectra and FT-IR spectra imply that the aromatic compounds present in the initial tannery effluent have been degraded to linear aliphatic compounds. The spectral detail reveals that the phenolic compounds have been fragmented under heterogeneous Fenton oxidation process.

### Influence of $\text{H}_2\text{O}_2$ on catalytic oxidation of organics in tannery effluent

The ability of Co-NPAC to utilize  $\text{H}_2\text{O}_2$  was determined by iodometric titration along with four control studies. The results revealed that the Co-NPAC has the maximum utilization of  $\text{H}_2\text{O}_2$ . This includes the decomposition of the constituents of tannery effluent by  $\text{H}_2\text{O}_2$ , decomposition by activated carbon and decomposition by  $\text{H}_2\text{O}_2$  at pH 3.5 and 7. Fig. S3 shows that the mineralization of tannery effluent by  $\text{H}_2\text{O}_2$  was only about 10% up to 7 hours, whereas the decomposition in the presence of NPAC was 13%. There was a sudden rise in the decomposition of  $\text{H}_2\text{O}_2$  in the initial period of reaction with NPAC which is due to

rapid adsorption of  $\text{H}_2\text{O}_2$  by NAPC. The effect of ferrous sulphate (Fenton oxidation) on decomposition was studied at pH 3.5 and the results show that the decomposition of  $\text{H}_2\text{O}_2$  was 58%. The decomposition of  $\text{H}_2\text{O}_2$  into hydroxyl radical and hydroxyl ion results in the formation of ferric hydroxide precipitation at pH7. Thus, the availability of active oxidant and iron species were reduced and thus, the decomposition rate of  $\text{H}_2\text{O}_2$  was reduced after 2 h. The decomposition of  $\text{H}_2\text{O}_2$  for the generation of hydroxyl radical and there by catalytic oxidation of dye laden wastewater by Co-NPAC was greater than that of other reaction conditions. The decomposition of  $\text{H}_2\text{O}_2$  was 60% at pH7, confirmed the catalytic behavior of  $\text{H}_2\text{O}_2$ .

### **Hydroxyl radical generation confirmation by Excitation -Emission Spectra**

Fig.12 shows that TPA exhibited a significant excitation spectra in the range between  $\lambda_{\text{exc}}$  310nm to 330nm, and emission spectra in the range between  $\lambda_{\text{emi}}$  420nm to 470nm. The maximum wavelength for the generation of hydroxyl radical was  $\lambda_{\text{exc}}$  and  $\lambda_{\text{emi}}$  at 320nm and 450nm respectively (see Fig.S4 and Fig.S5). This corroborates with the reported fluorescence spectrum of insitu generated hydroxyl radical<sup>26</sup>.

### **Reusability of Co-NPAC**

The results on reusability of Co-NPAC for 5 cycles for oxidation of dye laden wastewater are presented in Fig.13. The figure shows that the efficiency of Co-NPAC was consistent in first 3 cycles with an efficiency of 78% for the same volume of effluent and the efficiency was decreased to 75% and 74% respectively in 4<sup>th</sup> and 5<sup>th</sup> cycles. This is due to the accumulation of untreated/partially oxidized pollutants in the outer pore surface area of Co-NPAC. Therefore, the availability of the active sites was reduced significantly and thus degradation efficiency was decreased. Simultaneously, the ability of the catalysts to

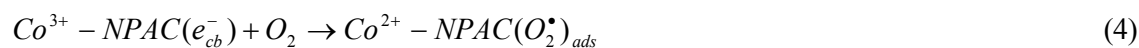
decompose  $H_2O_2$  into hydroxyl radical was studied for the same number of cycles. The study showed that decomposition of  $H_2O_2$  was 63% (Fig.S3). The percentage decomposition of  $H_2O_2$  was decreased in the fifth cycle compared to the first cycle. Hence, the Co-NPAC can be employed to generate hydroxyl radical for few cycles without regeneration and with consistent efficiency.

### Mechanistic view of mineralization of dye laden wastewater using Co-NPAC

The Co-NPAC was used as heterogeneous Fenton like catalyst to facilitate simultaneous adsorption and followed by degradation of dyestuff in wastewater. The cobalt oxide in NPAC was overlapped with oxygen and nitrogen functional groups of NPAC leaving behind unpaired electrons in 3d orbital of  $Co^{2+}$  and  $Co^{3+}$ . The unpaired electrons may serve to generate hydroxyl radicals from hydrogen peroxide, used as an oxidant in heterogeneous Fenton oxidation of dyestuff laden wastewater. The electron holes in Co-NPAC, which has been confirmed as an extrinsic semiconductor through energy gap value ( $E_g$ , 1.4 eV), generate hydroxyl radicals from hydrogen peroxide as per equation 2



Hydroxyl radicals are also generated from molecular oxygen explained as below. The molecular oxygen adsorb onto Co-NPAC matrix and form the reactive oxygen species using free electron in the matrix as shown below



The reactive oxygen species are reduced to hydroperoxy radicals using hydrogen ion present in the dye laden wastewater.



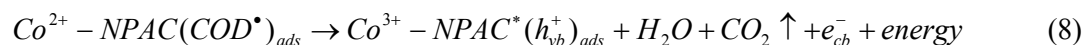
The hydroperoxy radicals generate hydroxyl radicals by  $H^+$  in wastewater



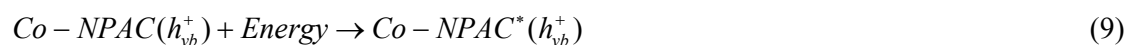
The electron holes in Co-NPAC serve to adsorb the organic substrate as expressed in terms of COD.



The adsorbed COD and hydroxyl radicals present at the proximate positions can undergo constructive overlapping to produce CO<sub>2</sub> and H<sub>2</sub>O, and regenerating back the virgin active site.



The energy is absorbed by the matrix itself and excites the matrix



Where  $h_{vb}^+$  is the electron hole in the valence band,  $e_{cb}^-$  is the electron in the conduction band, and Co-NPAC\* refers to the excited carbon active site

## Conclusion

The prepared and characterized cobalt oxide on nanoporous activated carbon could be used as a heterogeneous Fenton catalyst to generate hydroxyl radical using H<sub>2</sub>O<sub>2</sub>. The Co-NPAC was efficient enough to oxidize the organics (COD) present in the dye laden tannery effluent by 80%. The process parameters such as catalyst dosage, H<sub>2</sub>O<sub>2</sub> addition, pH and temperature were optimized as Co-NPAC, 1.5wt. %; H<sub>2</sub>O<sub>2</sub>, 10mM; pH, 7; and temperature, 30 °C. UV-Visible, Fluorescence and FT-IR spectroscopic analysis of tannery effluent before and after catalytic oxidation confirmed the oxidation of pollutants. The ability of the catalyst to generate hydroxyl radical from H<sub>2</sub>O<sub>2</sub> was also verified along with the radical generating capacity of Co-NPAC in 5 consecutive cycles. The Co-NPAC could be used for 5 cycles with COD removal efficiency by 75 to 80% in the heterogeneous Fenton treatment of tannery effluent.

## Notes

The authors declare no competing financial interest.

## Acknowledgements

One of the authors (S.K) acknowledges CSIR, India (grant number 31/6(365)/2012-EMR-I) for Senior Research Fellowship. The financial assistance under STRAIT network programme to carry out this work is highly acknowledged.

## S Supporting Information

Table S1 Pseudo second order kinetics corresponding  $k$  (rate of the reaction) and  $R^2$  values of different Co-NPAC, **Table S2** Pseudo second order kinetics of  $k$  (reaction rate) and  $R^2$  values at different  $H_2O_2$  concentrations, **Table S3** Pseudo second order kinetics of heterogeneous Fenton process corresponding  $k$  (reaction rate) and  $R^2$  value of different pH, **Table S4** Pseudo second order kinetics of heterogeneous Fenton process corresponding  $k$  (reaction rate) and  $R^2$  values at different temperature, **Fig. S3** Decomposition of hydrogen peroxide with different Fenton oxidation condition, Fig.S4 EES spectrum of terephthalic acid  $\langle\lambda\rangle$ excitation and  $\langle\lambda\rangle$ emission 315nm and 425nm, Fig.S5 2-hydroxy terephthalic acid using Co-NPAC/ $H_2O_2$  EES spectrum  $\lambda_{excitation}$ , 315nm;  $\lambda_{emission}$ , 425nm,

**References**

- [1] S.G. Schrank, H.J. Jose. *Chemosphere*. 2005, 60, 644–55.
- [2] T. Mandal, D. Dasgupta, S. Mandal, S. Datta, *J. Hazard. Mater.*, 2010, 180, 204–11.
- [3] S. Karthikeyan, M.E. Priya, R. Boopathy, M. Velan, A.B. Mandal, G. Sekaran, *Environ. Sci. Pollut. Res.*, 2012, 19(5),1828-1840.
- [4] G. Sekaran, S. Karthikeyan, K. Ramani, B. Ravindran, A. Gnanamani, A.B. Mandal, *Environ. Chem. Lett.* 2011, 9(4), 499-504.
- [5] G. Sekaran, S. Karthikeyan, R. Boopathy, P. Maharaja, V.K. Gupta, C. Anandan, *Environ. Sci. Pollut. Res.*, 2014, 21(2),1489-1502.
- [6] G. Sekaran, S. Karthikeyan, C. Evvie, R. Boopathy, P. Maharaja, *Clean Technol. Environ. Policy.*, 2013, 15(2), 245-253.
- [7] S. Karthikeyan, C.J. Magthalin, A.B. Mandal, G. Sekaran, *RSC Adv.*, 2014, 4(37), 19183-19195.
- [8] S. Karthikeyan, C.J. Magthalin, M. Mahesh, C. Anandan, G. Sekaran, *J. Chem. Tech. Biotechnol.*, DOI 10.1002/jctb.4403
- [9] S. Karthikeyan, G. Sekaran, *PCCP*. 2014, 16(9), 3924-3933.
- [10] R.M. Lattuada, C. Radtke, M.C.R. Peralba, J.H.Z. Santos Dos. *Water Air Soil Pollut.*, 2013, 224,1396.
- [11] S. Karthikeyan, C. Anandan, J. Subramanian, G. Sekaran . *RSC Adv.*, 2013, 3,15044–57.
- [12] Y. Li, J. Chen, J. Liu, M. Ma, W. Chen, L. Li, *J. Environ. Sci.*, 2010, 22(8), 1290–6.
- [13] A. Ward, C. Weber. *Chem.Cat.Chem.*, 2013, 5, 959–65.

- [14] X. Yang, P.F. Tian, C. Zhang, Y.Q. Deng, J. Xu, J. Gong, Y.F. Han, *Appl. Catal. B Environ.*, 2013, 134-135, 145–52.
- [15] Y. Hao, G. Hao, D. Guo, C. Guo, W. Li, M. Li. *Chem. Cat. Chem.*, 2012, 4, 1595–602.
- [16] P.R. Shukla, S. Wang, H. Sun, H. M. Ang, M. Tade. *Appl. Catal. B: Environ.*, 2010, 100, 529-534.
- [17] Q. Yang, H. Choi, Y. Chen, D.D. Dionysiou, *Appl. Catal. B. Environ.* 2008, 77, 300–307.
- [18] Q. Yang, H. Choi, D.D. Dionysiou, *Appl. Catal. B. Environ.* 2007, 74, 170–178.
- [19] W. Zhang, H.L. Tay, S.S. Lim, Y. Wang, Z. Zhong, R. Xu, *Appl. Catal. B. Environ.*, 2010, 95, 93–99.
- [20] J. Trawczynski, *Carbon*. 2003, 41(8), 1515-1523.
- [21] Q. Zhou, X. Wang, J. Liu, L. Zhang. *Chem. Eng. J.*, 2012, 200-202, 619–26.
- [22] Y. Chang Hun, Y.H. Park C.R. Park, *Carbon*, 2001, 39, 559
- [23] K.M. Kaprielova, I.I. Ovchinnikov, O.A. Yakovina, A.S. Lisitsyn. *Chem. Cat. Chem.* 2013, 520, 15–24.
- [24] S. Karthikeyan, A. Titus, A. Gnanamani, A.B. Mandal and G. Sekaran, *Desalination* 2011, 281, 438–445.
- [25] K. I. Ishibashi, A. Fujishima, T. Watanabe, K. Hashimoto, *Electrochem. Commun.*, 2000, 2(3), 207-210.
- [26] W. Liao, Y. Zhang, M. Zhang, M. Muruganatha, S. Yoshihara, *J. Phys. Chem. Solids*, 2013, 231, 455–63.

- [27] W. Yue, A.H. Hill, A. Harrison, W. Zhou, *Chem. Commun.*, 2007, 2518–2520
- [28] Y. Liu, G. Zhu, B. Ge, H. Zhou, A. Yuan, X. Shen, *Cryst.Eng.Comm.*, 2012, 14, 6264-6270.
- [29] H. M. Yang, J. Ouyang and A. D. Tang, *J. Phys. Chem. B.* 2007, 111,8006-8013.
- [30] M. Salavati-Niasari, N. Mir, F. Davar, *J. Phys. Chem. Solids.*, 2009, 70, 847-852
- [31] X. H. Xia, J. P. Tu, X.L. Wang, C.D. Gu and X.B. Zhao, *Chem. Commun.*, 2011, 47, 5786–5788.
- [32] C. Z. Zhu, S. J. Guo, Y. X. Fang and S. J. Dong, *ACS Nano.*, 2010,4, 2429–2437.
- [33] S. Karthikeyan, K. Viswanathan, R. Boopathy, P. Maharaja, G. Sekaran, *J. Ind. Eng. Chem.*, 2014, DOI: 10.1016/j.jiec.2014.04.036
- [34] B. Moon, Y. Park, K. Park. *Desalination*, 2011, 268, 249–52.
- [35] M. R. Silverstein, X. Francis, Webster and David Kiemle; USA; seventh edition; chapter 2; pp. 72-126.

Table 1 Characteristics of before and after Co-NPAC treated water

| S.No | Parameter                 | Raw wastewater | Co-NPAC Treated wastewater | Percentage removal |
|------|---------------------------|----------------|----------------------------|--------------------|
| 1    | PH                        | 6.1±0.64       | 5.8±0.92                   |                    |
| 2    | COD                       | 1740±436       | 382±110                    | 78                 |
| 3    | TOC                       | 610±198        | 120±69                     | 80.3               |
| 4    | BOD                       | 732±146        | 38±16                      | 94.8               |
| 5    | Sulphide                  | 9±6.4          | Nil                        | 100                |
| 6    | Sulfate                   | 1026±192       | 604±86                     | 41.1               |
| 7    | VFA                       | 1123±344       | 326±92                     | 71                 |
| 8    | Total Dissolved Solids    | 36642 ±262     | 21640 ± 232                | 41                 |
| 10   | Chloride                  | 9458 ± 220     | 8120 ± 128                 | 14.1               |
| 11   | Ammonia                   | 560 ± 58       | 96 ± 16                    | 82.8               |
| 12   | TKN                       | 746 ± 128      | 154 ± 44                   | 79.3               |
| 13   | Volatile Dissolved Solids | 2.1302         | 0.2160                     | 89.8               |
| 14   | Surfactant                | 12.3           | 0.96                       | 92.1               |

All values except pH and percentage reduction are expressed in mg/L.

**Table 2** Surface area, pore volume and average pore diameter of NPAC and Co-NPAC obtained from rice husk (determined by N<sub>2</sub> adsorption).

| Sample                                  | NPAC  | Co-NPAC |
|---|-------|---------|
| Total Surface area(m <sup>2</sup> /g)   | 153   | 52      |
| S <sub>meso</sub> (m <sup>2</sup> /g)   | 119   | 44      |
| S <sub>micro</sub> (m <sup>2</sup> /g)  | 34    | 7.9     |
| Total pore volume (cm <sup>3</sup> /g)  | 0.19  | 0.08    |
| V <sub>micro</sub> (cm <sup>3</sup> /g) | 0.017 | 0.004   |
| V <sub>meso</sub> (cm <sup>3</sup> /g)  | 0.17  | 0.079   |
| Average pore diameter (nm)              | 5     | 6       |

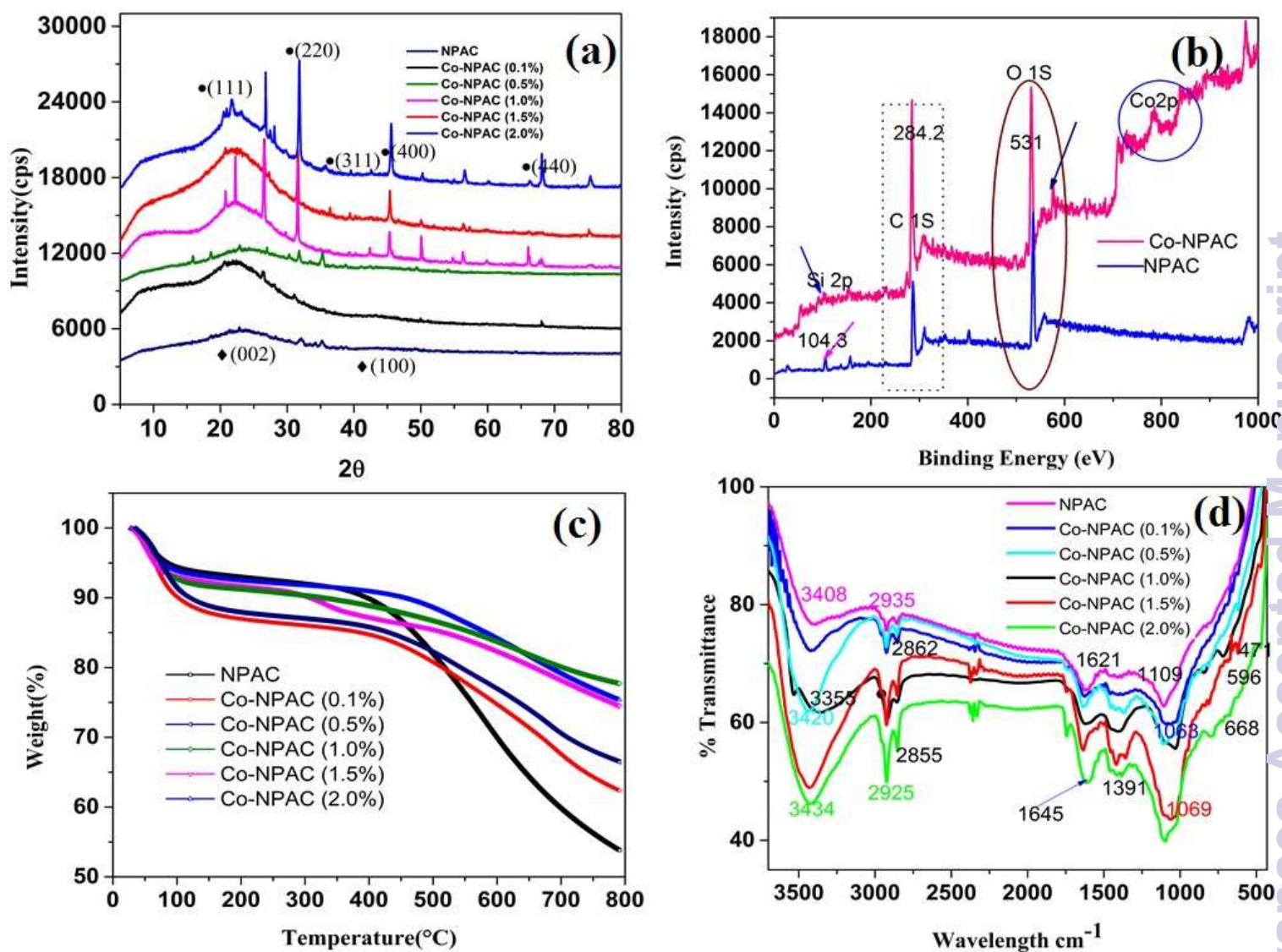


Fig. 1 (a) X-ray diffraction of patterns of NPAC and Co-NPAC, (b) X-ray photoelectron survey scan spectra of NPAC and Co-NPAC, (c) TGA spectra of NPAC and Co-NPAC, (d) FT-IR spectra of NPAC cobalt oxide in NPAC.

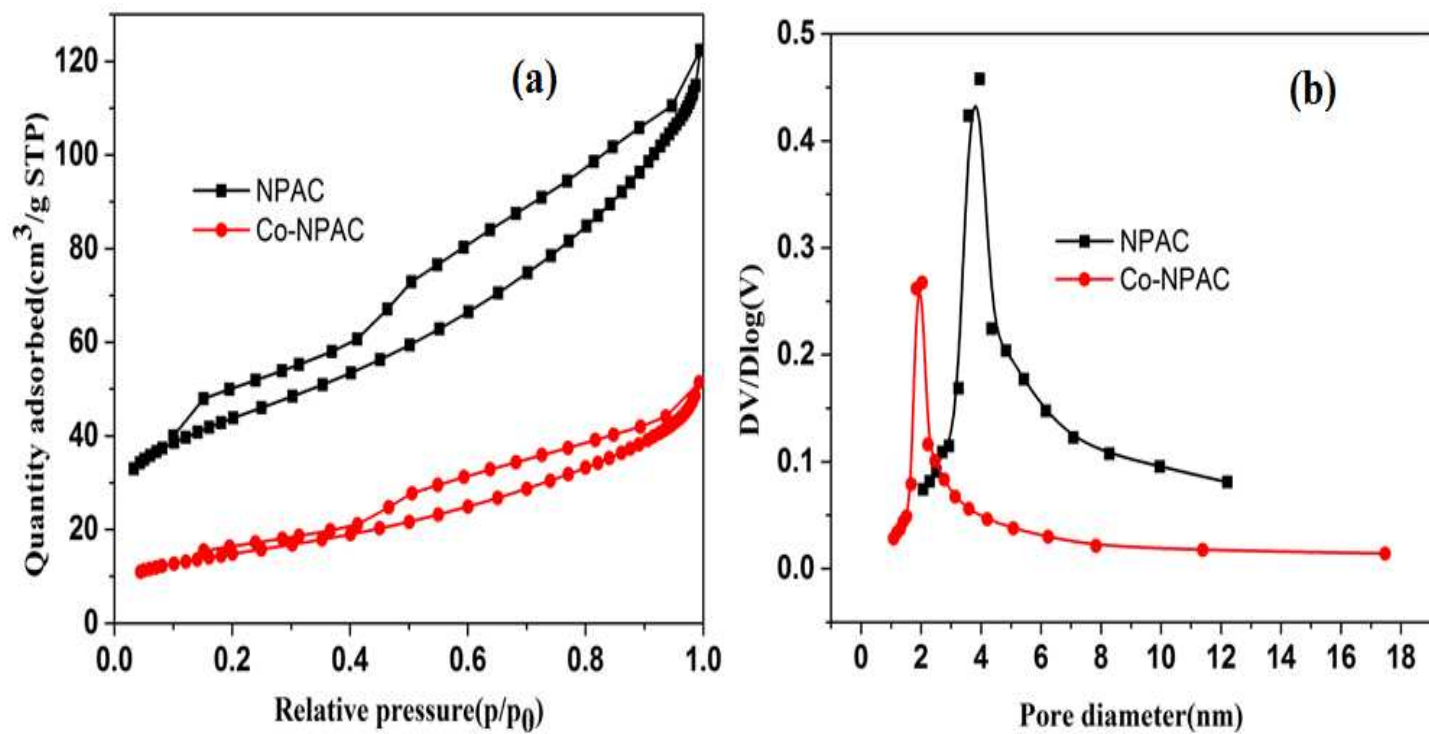


Fig. 2(a) Adsorption isotherm of NPAC and Co-NPAC samples, (b) pore size distribution of NPAC and Co-NPAC.

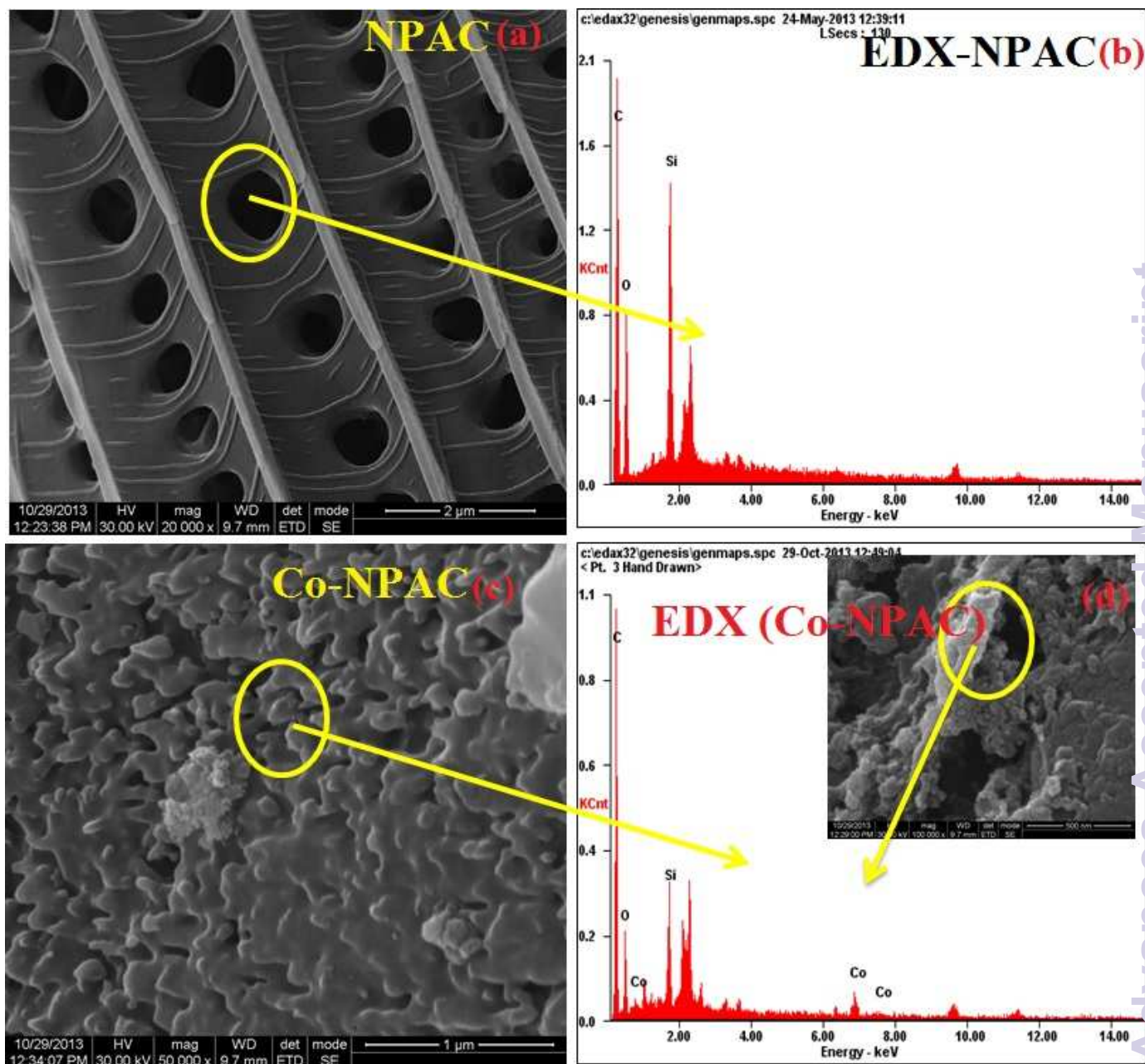


Fig. 3 (a) HR-SEM image of thermal-treated NPAC, (b) thermal-treated NPAC with corresponding EDX spectrum, (c) HR-SEM image of thermal-treated Co-NPAC, (d) Thermal-treated Co-NPAC with corresponding EDX spectrum.

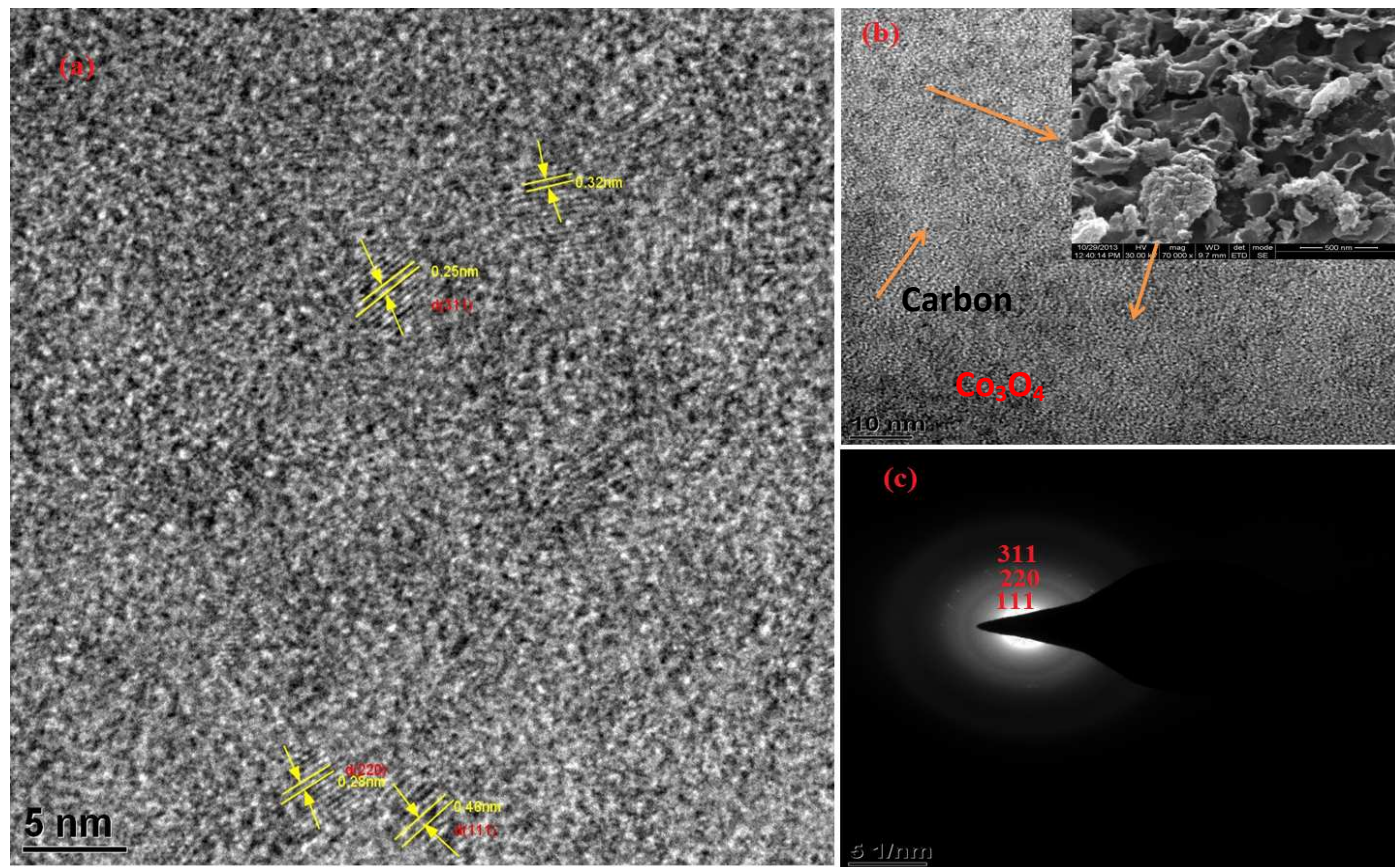


Fig. 4 (a,b) HR-TEM image of Co-NPAC, (c) SAED pattern of Co-NPAC

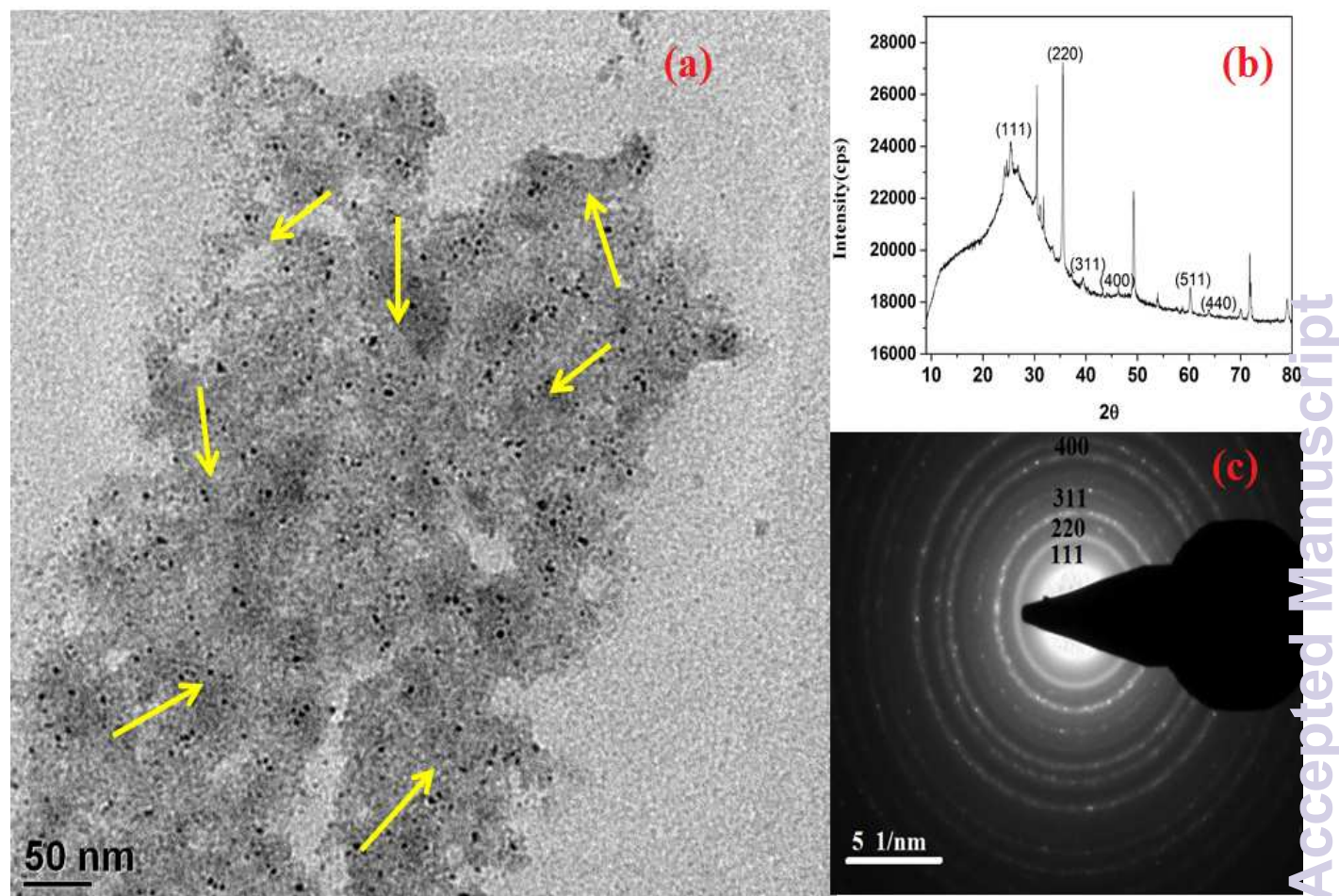


Fig. 5(a) HR-TEM image of Co-NPAC, (b) X-ray diffraction of patterns of Co-NPAC, (c) SAED pattern of Co-NPAC

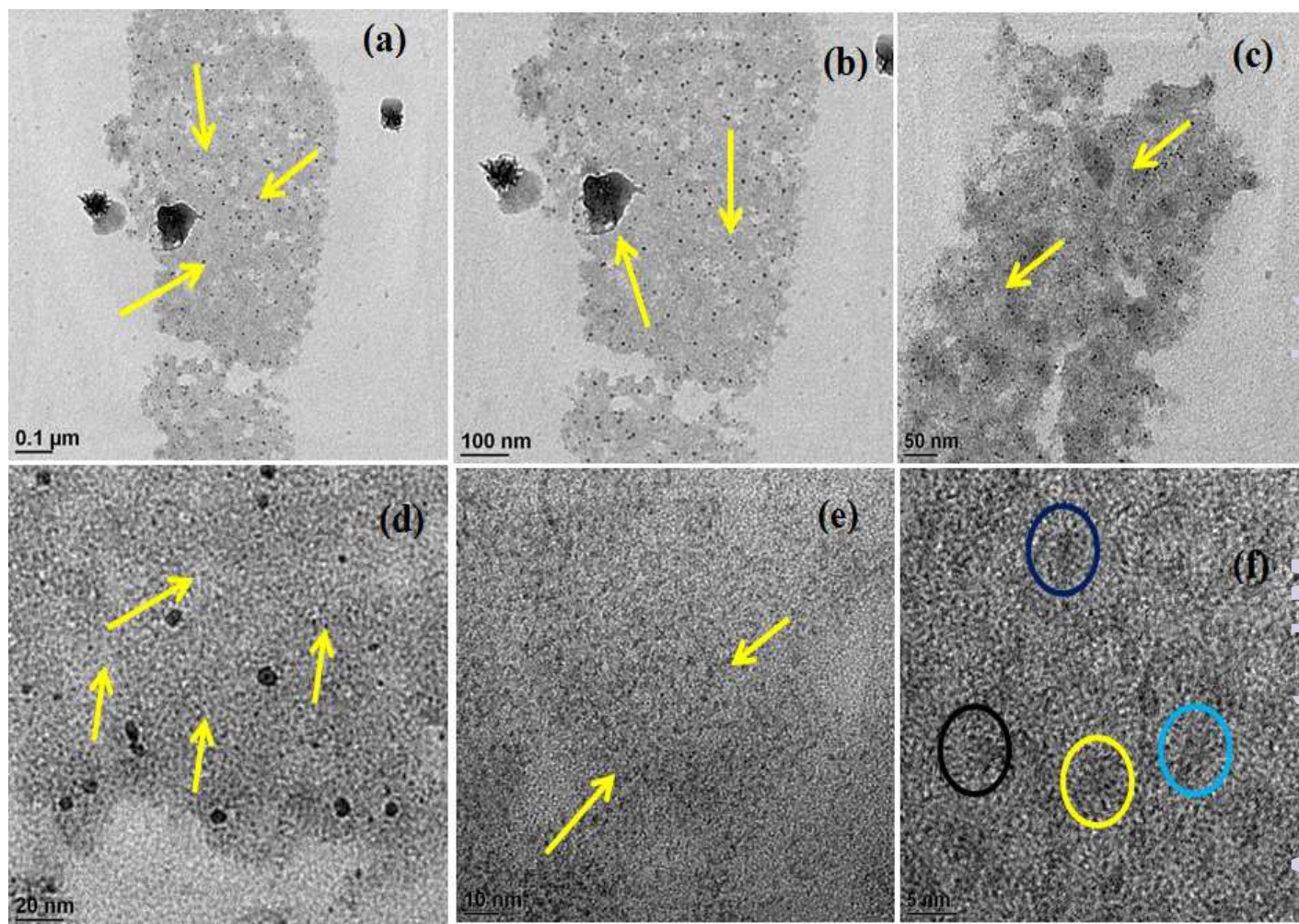


Fig. 6(a-f) HR-TEM image of Co-NPAC<sub>400</sub> at different nanometer intervals

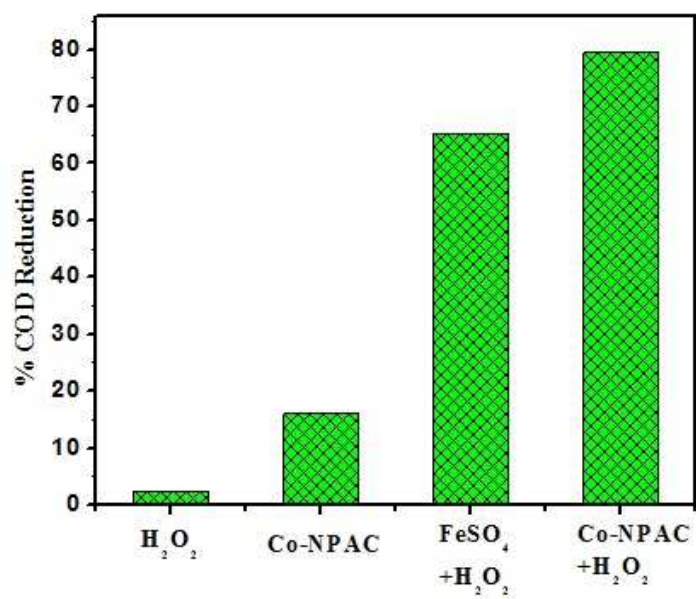


Fig. 7 Comparison of oxidation process of dye laden tannery wastewater

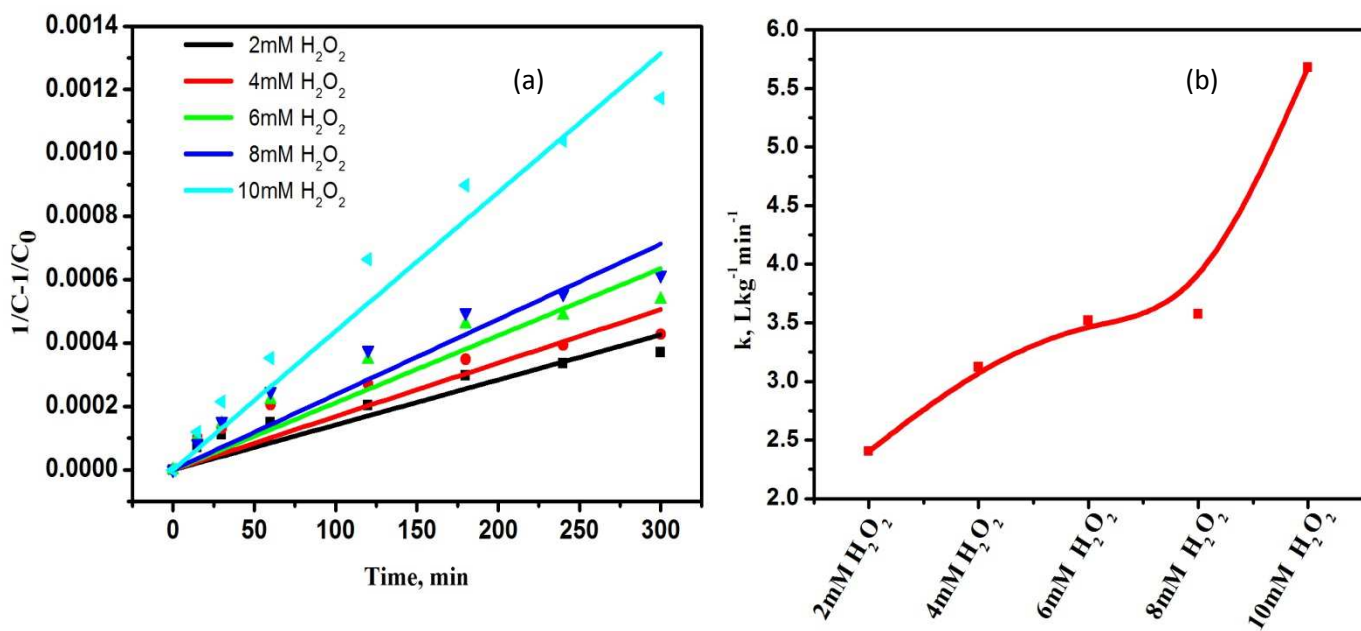


Fig. 8 Pseudo second order kinetics of Fenton process using different  $H_2O_2$  concentrations 1mM, 2mM, 3mM, 4mM and 5mM  $H_2O_2$ , a)  $1/C-1/C_0$  Vs time, t plot for all dosages, b) reaction rate behavior for varying concentration

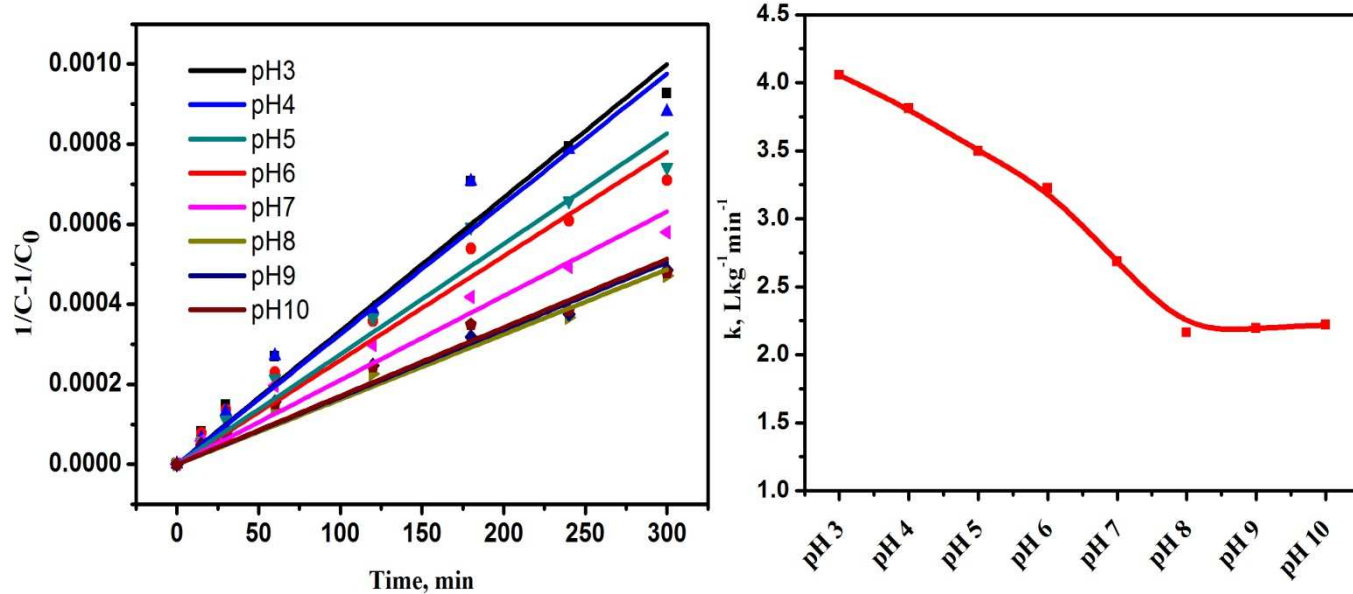


Fig. 9 Pseudo second order kinetics of heterogeneous Fenton process at different pH from pH 3 to 10, a)  $1/C-1/C_0$  Versus time,  $t$  plot at pH 3 to 10, b) reaction rate at pH 3 to 10, c) corresponding  $k$  (reaction rate) and  $R^2$  value at different pH conditions.

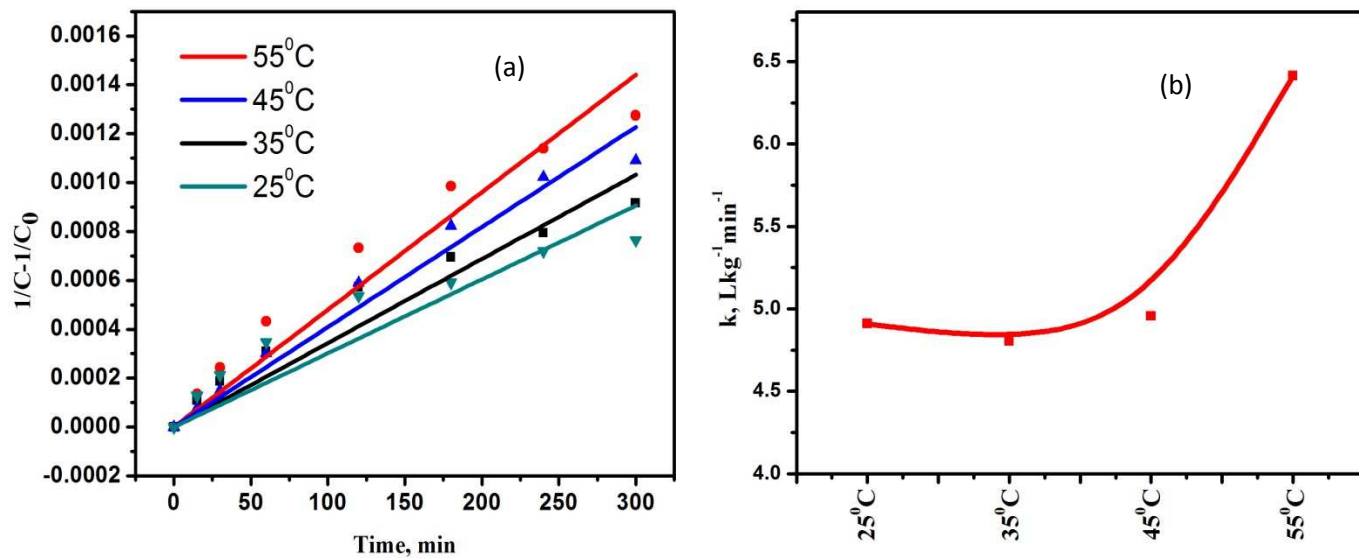


Fig. 10 Pseudo second order kinetics of Fenton process at different temperatures 25 °C, 35 °C, 45 °C and 55 °C; a)  $1/C-1/C_0$  Versus time,  $t$  plot for all temperatures b) reaction rate behavior at different temperatures, c) reaction rate constant  $k$  and  $R^2$  value at different temperatures.

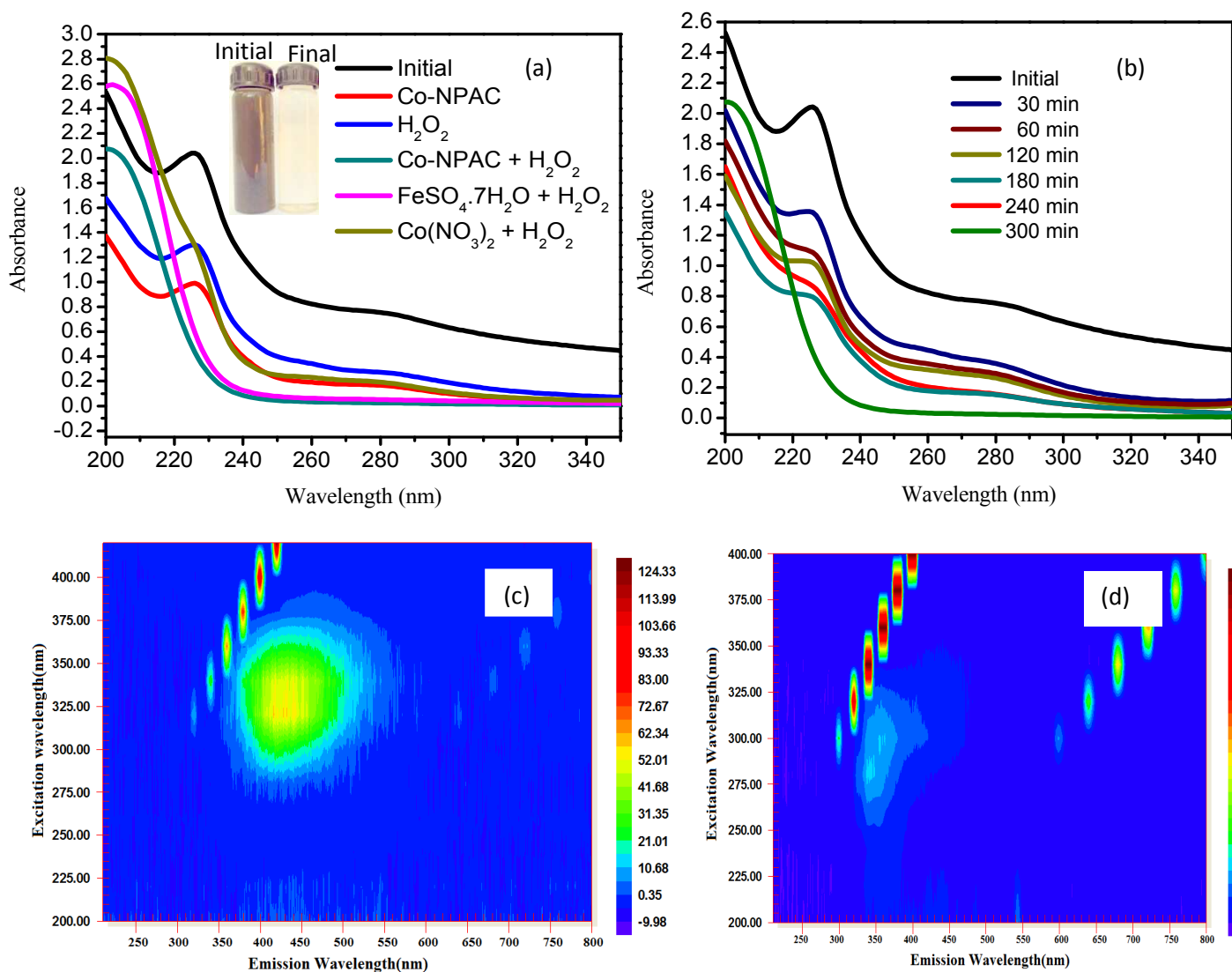


Fig.11 UV-Visible spectra of dye laden wastewater before and after Fenton a) different oxidation, (b) different time intervals, (c) Excitation and Emission Spectra (EES) of initial tannery effluent in the range of  $\lambda_{exi}$  of 200 to 400 nm and  $\lambda_{emi}$  of 210 to 800 nm. (d) EES for heterogeneous Fenton oxidized samples

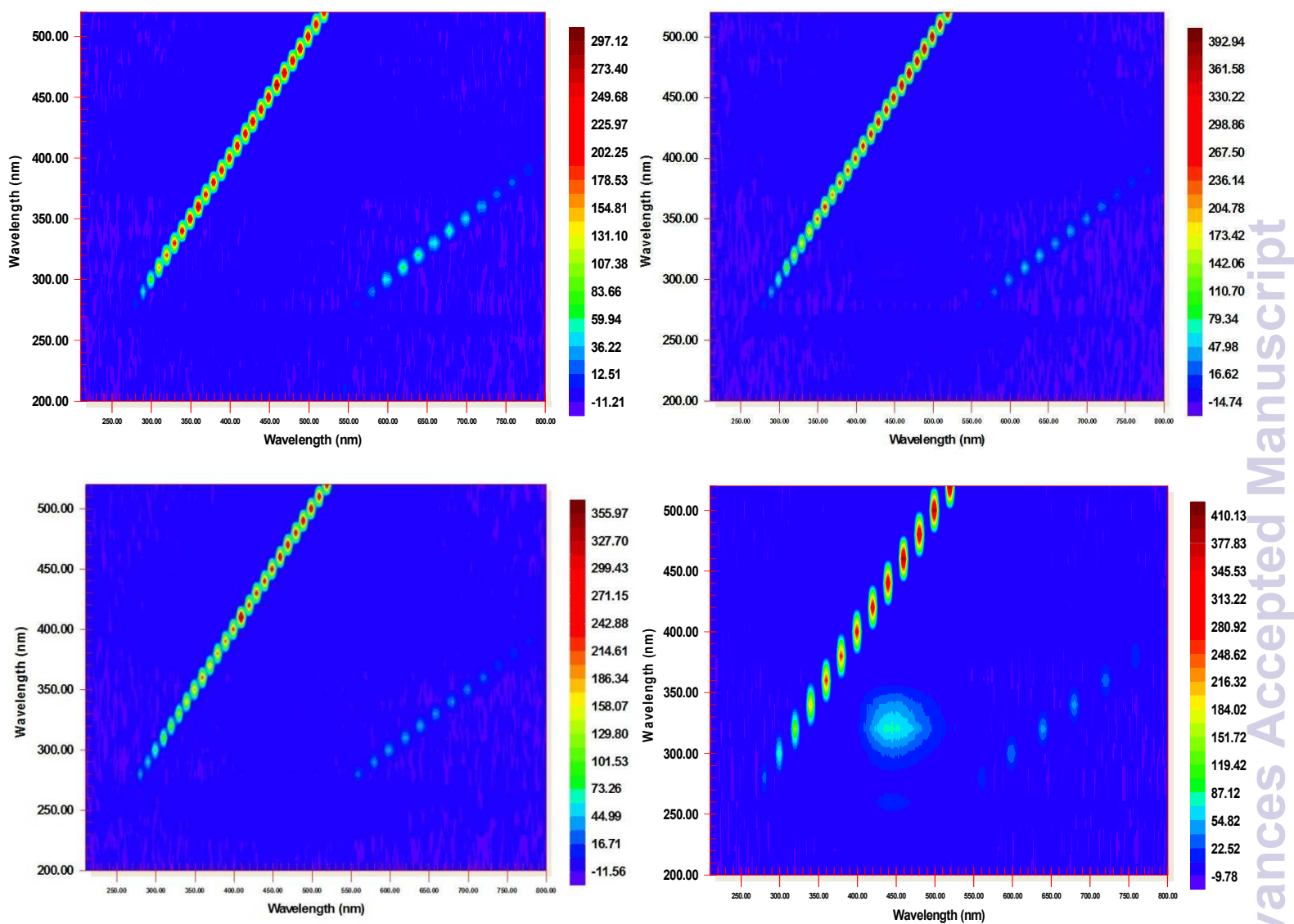


Fig. 12 (a)Terephthalic acid, (b)Terephthalic acid with  $H_2O_2$ , (c) Terephthalic acid with Co-NPAC, (d)Terephthalic acid with Co-NPAC and  $H_2O_2$

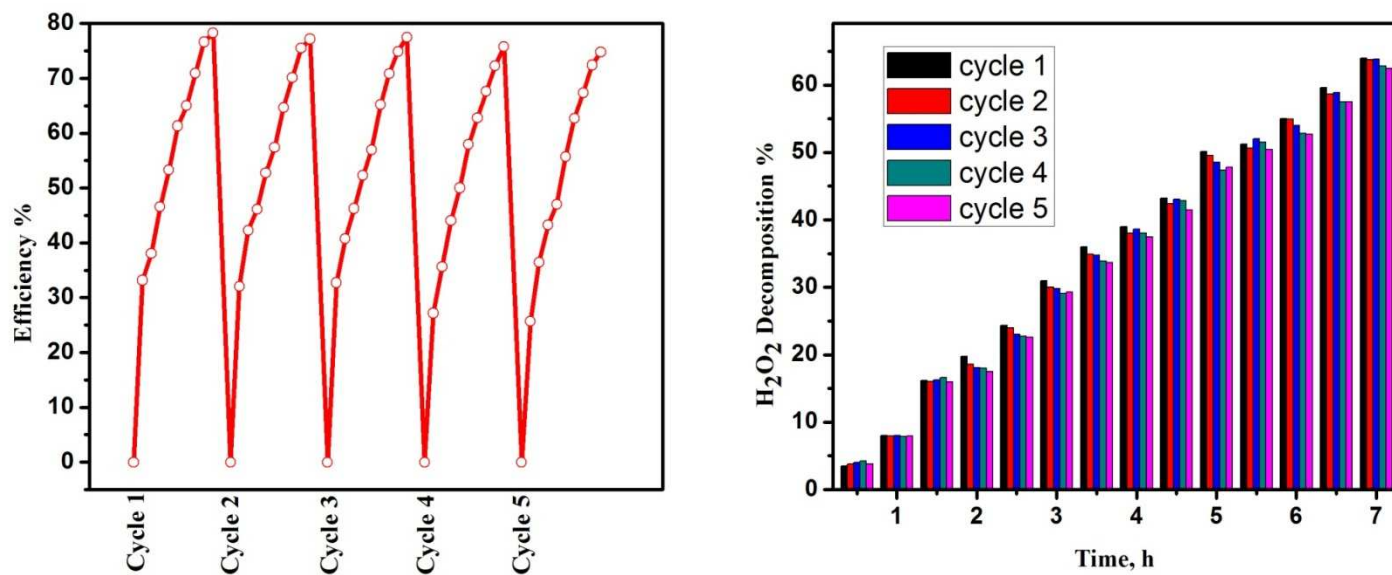


Fig. 13 Variation COD reduction efficiency during Fenton oxidation process, (b) decomposition

H<sub>2</sub>O<sub>2</sub> by Co-NPAC for 5 numbers of continuous cycles.